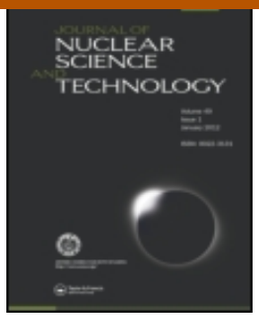

Journal of Nuclear Science and Technology

ISSN: 0022-3131 (Print) 1881-1248 (Online) Journal homepage: https://www.tandfonline.com/loi/tnst20

Unfolding Method with X-ray Path Length-Dependant Response Functions for Computed Tomography Using X-ray Energy Information

Ryo IMAMURA , Kenta MIKAMI , Yuko MINAMI , Ikuo KANNO , Masahiko OHTAKA , Makoto HASHIMOTO , Kuniaki ARA & Hideaki ONABE

To cite this article: Ryo IMAMURA , Kenta MIKAMI , Yuko MINAMI , Ikuo KANNO , Masahiko OHTAKA , Makoto HASHIMOTO , Kuniaki ARA & Hideaki ONABE (2010) Unfolding Method with X-ray Path Length-Dependant Response Functions for Computed Tomography Using X-ray Energy Information, Journal of Nuclear Science and Technology, 47:11, 1075-1082, DOI: 10.1080/18811248.2010.9711672

To link to this article: https://doi.org/10.1080/18811248.2010.9711672

Published online: 05 Jan 2012.

Journal of NUCLEAR SCIENCE and TECHNOLOGY, Vol. 47, No. 11, p. 1075–1082 (2010)

ARTICLE

Unfolding Method with X-ray Path Length-Dependant Response Functions for Computed Tomography Using X-ray Energy Information

Ryo IMAMURA[1,*], Kenta MIKAMI[1,†], Yuko MINAMI[1], Ikuo KANNO[1], Masahiko OHTAKA[2], Makoto HASHIMOTO[2], Kuniaki ARA[2] and Hideaki ONABE[3]

[1]*Graduate School of Engineering, Kyoto University, Sakyo, Kyoto 606-8501, Japan*
[2]*O-arai Research and Development Institute, Japan Atomic Energy Agency, Narita, O-arai, Ibaraki 311-1393, Japan*
[3]*Raytech Corporation, Yoto, Utsunomiya 321-0904, Japan*

(Received April 24, 2010 and accepted in revised form May 19, 2010)

The computed tomography (CT) values obtained by the energy subtraction method with a transXend detector, which measured X-rays as current and gave the corresponding X-ray energy information, show the disadvantage that the CT values are dependent on the thickness of a homogeneous phantom. In order to obtain constant CT values for a uniform material, a new unfolding method is proposed using variable response functions of the transXend detector according to the X-ray path length in the phantom. The CT values measured using the new unfolding method are discussed with respect to the energy range used in the unfolding process, the number of segment detectors, and the substrate of the segment detectors.

KEYWORDS: X-rays, energy subtraction, unfolding, energy measurement, contrast media, CT, transmission tomography, beam hardening, photon detector

I. Introduction

When a polychromatic X-ray beam is incident upon a material, high-energy X-rays will dominate the energy spectrum of the transmitted X-ray beam since all materials attenuate low-energy X-rays more strongly than high-energy X-rays. This phenomenon is called the beam hardening effect.[1)] In X-ray computed tomography (CT), the beam hardening effect makes the observation of cancer tumors difficult when the subject area is thick, even though the cancer tumor is marked by contrast media. In our previous study, measurements of X-ray energy and the application of the energy subtraction (ES) method were shown to be effective for avoiding the beam hardening effect.[2)]

The conventional method for measuring X-ray energies is, however, not suitable for a practical CT measurement as the limited counting rate of X-ray detectors requires a long acquisition time to obtain the X-ray energy spectrum. To bring the ES X-ray CT into practical use, we invented a detector that measures X-rays as current, from which the X-ray energy distribution is then determined.[3)] This detector, named the transXend detector, consists of several segment detectors, which are aligned along the line of X-ray incidence. The measured current values and response functions are used to obtain the X-ray energy distribution by the unfolding method.

We employed the transXend detector with CsI(Tl) scintillator as the segment detectors to make CT measurements on a cylindrical acrylic phantom with a 40-mm-diameter and 10-mm-diameter iodine region in the center.[4)] Although the CT values in the iodine contrast region of the phantom were larger than the ones obtained by a conventional current measurement CT, the CT values in the homogeneous acrylic region were dependent on the thickness of acrylic through which the X-rays passed before interacting with the detector. This defect was the result of an insufficient unfolding method, because the CT values in the acrylic region were constant when the energy of each X-ray was measured as shown in Fig. 12 in the literature.[2)]

In this paper, we propose an improved unfolding method to obtain a constant CT value for a homogeneous material. In the new method, the response functions used in the unfolding process are modified as a function of the X-ray path length within the phantom. The experiments to obtain the response function as a function of the X-ray path length are carried out using the transXend detector with the segment detectors made of Si(Li). CT images acquired using Si(Li) segment detectors are compared with those obtained using CsI(Tl) segment detectors. Additionally, we discuss the dependence of CT values from the viewpoints of the number of segment detectors and the energy range of interest.

II. Brief Description of the TransXend Detector

A schematic drawing of the transXend detector is shown in **Fig. 1**. The transXend detector consists of several segment detectors (each is subsequently referred to as a

*Corresponding author, E-mail: c-puyo1@nucleng.kyoto-u.ac.jp
†Present address: *Fuji Electric Systems Co., Ltd., 1 Fuji-machi, Hino, Tokyo 191-8502, Japan*

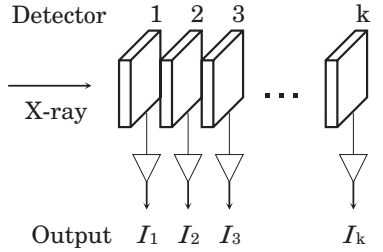

Fig. 1 Schematic drawing of the transXend detector

Table 1 Assigned energy ranges (keV)

	E_1	E_2	E_3	E_4	E_5	E_6
80 kV	20–27	27–33	33–39	39–50	50–65	65–80
100 kV	20–27	27–33	33–39	39–60	60–80	80–100
120 kV	20–27	27–33	33–39	39–60	60–90	90–120

channel), which are aligned along the line of X-ray incidence. Low-energy X-rays tend to be absorbed by the forward segment detectors. Although high-energy X-rays can be absorbed in the forward segment detectors, some of them arrive at the backward segment detectors where they are absorbed. The relationship between the measured current and the X-ray energy distribution is expressed as:

$$\begin{pmatrix} I_1 \\ I_2 \\ \vdots \\ I_k \end{pmatrix} = \begin{pmatrix} R_{1,1} & R_{1,2} & \cdots & R_{1,n} \\ R_{2,1} & R_{2,2} & & \vdots \\ \vdots & & \ddots & \\ R_{k,1} & \cdots & & R_{k,n} \end{pmatrix} \begin{pmatrix} Y_1 \\ Y_2 \\ \vdots \\ Y_n \end{pmatrix}, \quad (1)$$

where I_i is the current value measured by the ith channel detector, $R_{i,j}$ ($i = 1, k$, $j = 1, n$) is the response function of the ith channel detector for the X-rays with energy range, E_j, as indicated in **Table 1**, and Y_j is the incident X-ray event in E_j. Each $R_{i,j}$ is unfolded by using the SAND II code,[5] which is an iterative method for calculation of the least-square value of a logarithm. A detailed method for obtaining the response function is described in the literature.[3]

For the demonstration of the operating principle of the transXend detector, the response function is determined using a rectangular acrylic phantom, *i.e.*, in the case of constant X-ray path length.[3] When a CT image is reconstructed with the response function described above, the obtained CT values for a homogeneous material show dependence on the X-ray path length in the phantom.[4] This indicates that response functions as a function of X-ray path length are necessary for the unfolding process. We describe the method of obtaining response functions as a function of X-ray path length for CT measurements in the following section.

III. Experiments

1. Experimental Setup for Response Function Acquisition

The experimental setup is shown in **Fig. 2**. X-rays from the X-ray tube (TRIX-150S, Toreck Co., Ltd., Japan) are

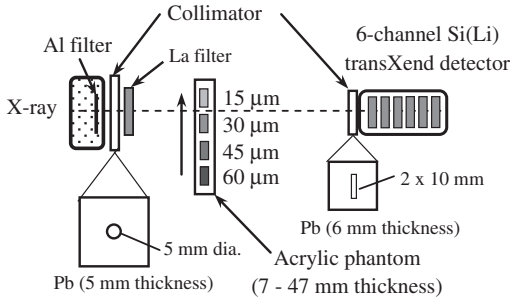

Fig. 2 Experimental setup of the X-ray tube, filters, acrylic phantom, and transXend detector

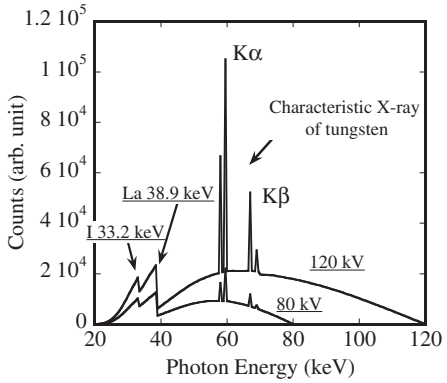

Fig. 3 Calculated energy spectra of the X-rays for tube voltages of 80 and 120 kV after transmission through a La filter (100 μm thick), acrylic phantom (40 mm thick), and iodine region (30 μm thick)

first transmitted through an Al filter (2 mm thickness), a Pb collimator (5 mm diameter, 5 mm thickness), and a La filter (100 μm thickness). The Al filter is inserted to absorb low-energy X-rays (<20 keV), as X-rays of this energy provide no useful information inside the phantom (or analogously to clinical practice, the human body), thus they contribute only to undesirable exposure dose. The La filter is inserted to decrease the amount of high-energy X-rays (>40 kV), which are only weakly attenuated by iodine contrast media, and to increase the steepness of the X-ray energy spectrum around the K-edge of iodine.

Typical energy spectra of X-rays are calculated and are shown in **Fig. 3** for the tube voltages of 80 and 120 kV. The sharp peaks around 60 and 67 keV are the characteristic X-rays of tungsten, which is used as the electron beam target in the X-ray tube. The X-rays are attenuated strongly above the K-edges of iodine (33.2 keV) and La (38.9 keV).

The transXend detector has 6 Si(Li) segment detectors. The dimensions of each segment detector are $10 \times 10 \times 1\,\text{mm}^3$. The detector is operated at room temperature without applying a bias voltage as the mean free paths of electrons and holes in silicon are sufficiently long enough to arrive at each electrode. Output signals are amplified with a six-channel current preamplifier (IPA-6, Raytech Corp., Japan) and read simultaneously using timer counters with voltage-frequency converters (VFCT-8S4, Laboratory Equipments Corp., Japan). A 7-mm-thick rectangular acrylic phantom

contains four regions of iodine contrast media with the effective iodine thicknesses of 15, 30, 45, and 60 µm. Slabs of 10-mm-thick acrylic are incrementally added to the rectangular phantom to produce a total acrylic phantom thickness ranging from 7 to 47 mm, since the X-ray path length in the 40-mm-diameter acrylic phantom is changed from 0 to 40 mm. The position of the acrylic phantom is changed by a precision stage to allow the measurement of current values for each iodine thickness. The measurements were conducted at X-ray tube voltages of 80, 100, and 120 kV, and at a tube current of 2 mA.

2. CT Measurements

For the CT measurements, the rectangular acrylic phantom shown in Fig. 2 is replaced with the cylindrical 40-mm-diameter acrylic phantom. The center of the phantom contains a 10-mm-diameter region filled with diluted iodine. The X-rays pass through 10-µm-thick iodine when they proceed the 10 mm distance in the diluted iodine region. The phantom is translated along the x-axis over a distance of 44.4 mm (moving 112 times in 0.4 mm increments). The phantom is then rotated (θ) 30 degrees. The translation and rotation are repeated 6 times until the phantom has been rotated 180 degrees from the initial orientation. The acquired data are duplicated 2 times to have the data in 10 degree intervals.

IV. Analysis

1. Response Function

The measured current values in Sec. III-1 are fitted with an exponential function by the least-squares method to get interpolated current values versus acrylic thickness for various iodine thicknesses and segment detectors, as shown in **Fig. 4**. The interpolated current values are used to calculate the response functions as a function of the acrylic thickness. Response functions are determined for each acrylic thickness by the same method as described in the literature.[3] The response functions for acrylic thicknesses of 0 to 47 mm are acquired in 1 mm intervals and are used to change the X-ray path length within the cylindrical acrylic phantom.

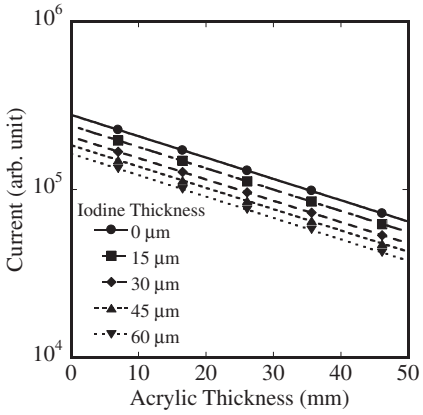

Fig. 4 Exponential fit of the current values measured by the 1st channel detector. The X-ray tube voltage was 100 kV.

2. Unfolding Method

Using the SAND II code, the X-ray energy distribution, Y_j, is determined using the measured current values, the response functions, and an initial guess of the X-ray energy distribution. The initial guess of the X-ray energy distribution is calculated as follows.

The energy spectrum of X-rays, $\Psi_0(E)$, emitted by the bombardment of electrons with acceleration voltage E_0 to a target is written as

$$\Psi_0(E)dE = const. \times Z\frac{E_0 - E}{E}dE, \tag{2}$$

where Z is the atomic number of the target and E is the energy of the X-rays.[6] With absorbers between the X-ray source and detector, the spectrum of incident X-rays, $\Psi(E)$, to the detector is given as

$$\Psi(E)dE = \Psi_0(E) \cdot \exp\left\{-\sum_m \left(\frac{\mu_m}{\rho_m} \times t_m \times \rho_m\right)\right\}dE, \tag{3}$$

where μ_m/ρ_m is the mass attenuation coefficient, t_m is the thickness, and ρ_m is the density of the material m.

The initial guess of the X-ray energy distributions, Y_j, is prepared for various iodine thicknesses with acrylic thickness estimated from the CT image at (x, θ) measurement point obtained by the conventional current measurement method. The difference between the measured current value, I_i $(i = 1, 6)$, and the calculated current value $\sum_{j=1}^{6} R_{i,j}Y_j$ is expressed as

$$\sigma = \sqrt{\frac{1}{5}\sum_{i=1}^{6}\left(\frac{\sum_{j=1}^{6} R_{i,j}Y_j}{I_i} - 1\right)^2}. \tag{4}$$

The energy distribution, Y_j $(j = 1, 6)$, for the measurement point (x, θ) is determined using the SAND II code to have the minimum σ. CT images with X-ray energy information are reconstructed with obtained X-ray events, Y_2 and Y_3, for which energies are slightly below and above the iodine K-edge, respectively.

V. Results and Discussion

1. Iodine Thickness Estimation with Two Different Response Functions

To demonstrate that a response function should be chosen according to the X-ray path length in the phantom, the iodine thicknesses in a 40-mm-thick phantom were estimated using response functions made for two different acrylic thicknesses, 20 and 40 mm. Iodine thickness estimates were calculated using response functions for 20 mm (dashed line) and 40 mm (solid line) acrylic thicknesses and are shown in **Fig. 5**. The estimate of iodine thickness calculated using the response function made for the 40 mm acrylic thickness showed excellent agreement with the actual iodine thickness. When applying the response function made for 20 mm acrylic thickness for 40-mm-thick phantom, the X-ray absorption by the additional 20 mm of acrylic was regarded as absorp-

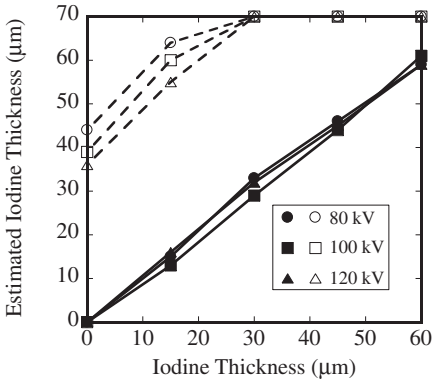

Fig. 5 Iodine thickness estimation for the 40-mm-thick acrylic phantom. The employed response functions were the ones obtained for a 40-mm-thick phantom (solid symbols) and for a 20-mm-thick phantom (open symbols).

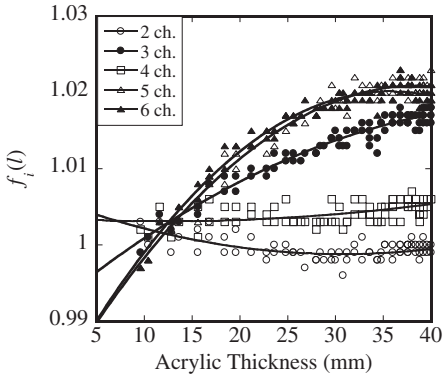

Fig. 6 Correction function $f_i(l)$ for each channel detector as a function of X-ray path length, l. The X-ray tube voltage was 100 kV.

tion by iodine. As a result, the estimated iodine thickness was more than the actual thickness. When the wrong response function was used (*i.e.*, the response function made for the 20 mm acrylic thickness), the resulting estimate of iodine thickness was significantly different from the actual iodine thickness. These results indicated that it was necessary to employ the response functions designed for the acrylic thickness closest to the X-ray path length.

2. Scatter Correction for Cylindrical Phantom

The incident X-rays were scattered by the cylindrical acrylic phantom differently than by the rectangular phantom. The difference in scatter by the two phantoms resulted in a difference between the measured current value, $I_{cyl,i}(l)$ at the ith channel detector for the cylindrical phantom, and the current value obtained by the measurement of the rectangular phantom (shown in Fig. 2) used for the acquisition of the response function, $I_{rect,i}(l)$. Before the CT measurements, a blank cylindrical acrylic phantom with the same diameter, which is subsequently called the reference phantom, was scanned to correct the difference as a function of X-ray path length, l. The current value obtained by measuring the reference phantom, $I_{ref,i}(l)$, was divided by $I_{rect,i}(l)$ to get the current ratio for the case of X-rays transmitted through the same path length, l. The correction function, $f_i(l)$, was obtained by normalizing with the current ratio for channel 1.

$$f_i(l) = \frac{I_{ref,i}(l)/I_{rect,i}(l)}{I_{ref,1}(l)/I_{rect,1}(l)}. \tag{5}$$

As shown in **Fig. 6**, the value $f_i(l)$ was less than 2% and was approximated with a quadratic function for each channel. The corrected current value, $I_{cor,i}(l)$, was obtained by dividing $I_{cyl,i}(l)$ by $f_i(l)$ according to:

$$I_{cor,i}(l) = I_{cyl,i}(l)/f_i(l). \tag{6}$$

Reduction of the scatter effect was confirmed when the aperture of the collimator on the detector was narrowed. The experiments were, however, conducted without changing the size of the collimator aperture to obtain enough current.

3. Energy-Based CT and Energy-Subtraction-Based CT

To obtain the X-ray path length at each (x, θ) measurement point, a CT image reconstructed with the current value was utilized. The X-ray energy distribution was unfolded by the SAND II code choosing response functions according to the X-ray path length obtained for (x, θ) measurement point at 1 mm intervals.

Energy-based CT and ES-based CT images were reconstructed using Y_3 and Y_2/Y_3, respectively. The energy-based CT corresponds to a quasi-monochromatic energy X-ray CT. The current-based, energy-based, and ES-based CT images acquired at tube voltages of 80, 100, and 120 kV are shown in **Fig. 7**. The CT value profiles on the center line of the phantom are shown in **Fig. 8** (the energy-based CT values were multiplied by -1 for clarity). In the current-based CT, the difference between the CT values in the acrylic and iodine regions decreased as the tube voltage increased. This happened because the X-ray attenuation coefficient of iodine decreased more than the attenuation coefficient of acrylic as the photon energy increased. As a result, the difference between the energy-averaged X-ray attenuation coefficient of iodine and that of acrylic became smaller. On the other hand, the differences in both the energy-based and ES-based CT were constant despite the increasing tube voltage. Moreover, at the tube voltage of 120 kV, the difference between the CT values in the iodine and acrylic regions in the energy-based and ES-based CT was twice as much as in the current-based CT. This meant that in energy-based and ES-based CT, the contrast media could be identified more clearly than in the current-based CT, especially at higher tube voltage. Conversely, the differences between the CT values in the iodine and acrylic regions measured with energy-based and ES-based CT were similar to the differences observed in the current-based CT at a tube voltage of 80 kV. This is because there was not much beam hardening within the small phantom at low tube voltages. In other words, when a thicker phantom was employed, the advantages of the energy-based and ES-based CT became apparent.

The ES-based CT image was also obtained by subtracting the energy-based CT image reconstructed with Y_3 data from the image reconstructed with Y_2 data. The X-ray attenuation coefficient of acrylic in the energy range of E_2 was almost

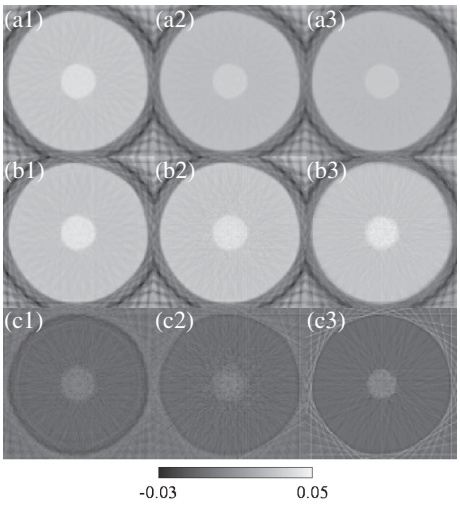

Fig. 7 (a) Current-based, (b) energy-based, and (c) ES-based CT images. The X-ray tube voltages were (1) 80, (2) 100, and (3) 120 kV.

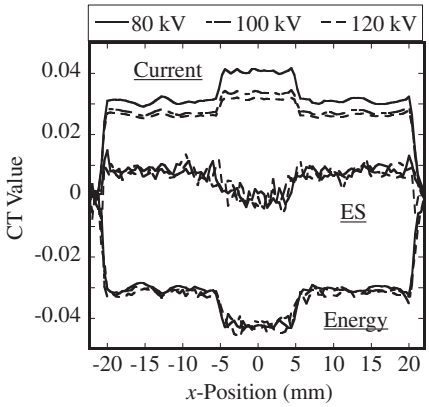

Fig. 8 CT value profiles on the center line of the phantom of the current-based, energy-based, and ES-based CT images (the energy-based CT values were multiplied by −1 for clarity)

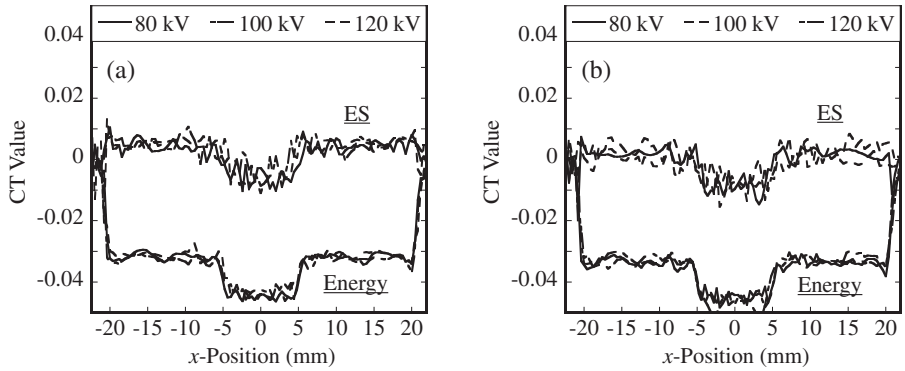

Fig. 9 CT value profiles on the center line of the phantom of the energy-based and ES-based CT images (the energy-based CT values were multiplied by −1 for comparison with Fig. 8). The energy ranges E_2 and E_3 were changed to (a) a half (30–33 and 33–36 keV) and to (b) a quarter (31.5–33 and 33–34.5 keV) of the original energy ranges.

equal to the one in the energy range of E_3. Consequently, the CT values measured with ES-based CT in the acrylic region were mostly zero, while the CT values in the iodine region were emphasized.

4. Energy Range Dependence of CT Values

To study the energy range dependence of the CT values, the energy ranges E_2 and E_3 were changed into a half and into a quarter, respectively. The energy ranges E_2 and E_3 are redefined as 30–33 and 33–36 keV for the half-energy range, and 31.5–33 and 33–34.5 keV for the quarter-energy range. Response functions were obtained and the data were analyzed by the same method as described in Sec. II for redefined energy ranges. The CT value profiles of the energy-based and ES-based CT are indicated in **Fig. 9** (the energy-based CT values were multiplied by −1 to allow comparison with Fig. 8). Compared with Fig. 8, it was apparent that the difference between the CT values in the acrylic region and in the iodine region became larger. In the ES-based CT measurement, the CT values in the acrylic region became closer to zero as the energy range narrowed.

5. Fluctuations of CT Values

The standard deviation, δ, of CT values is expressed as

$$\delta = \sqrt{\frac{\sum_{r=1}^{m}(a_r - \bar{a})^2}{m-1}}, \tag{7}$$

where a_r is a CT value at data point, r, $\bar{a}$ is the average of the CT values, and m is the number of data points. The averages and standard deviations of the CT values in the acrylic and iodine regions are shown in **Fig. 10** by columns and error bars, respectively. The standard deviations of the energy-based and ES-based CT values were larger than those of current-based CT values: the X-ray energy distributions were obtained as a result of calculations, while the current values were measured raw data. However, it could be said that the energy-based CT was better than the ES-based CT in terms of less fluctuation due to fewer calculations. In addition, the fluctuation of CT values increased as the energy ranges E_2 and E_3 were narrowed. In the current-measurement-based CT, the standard deviation decreased as the X-ray tube voltage increased, since the current values

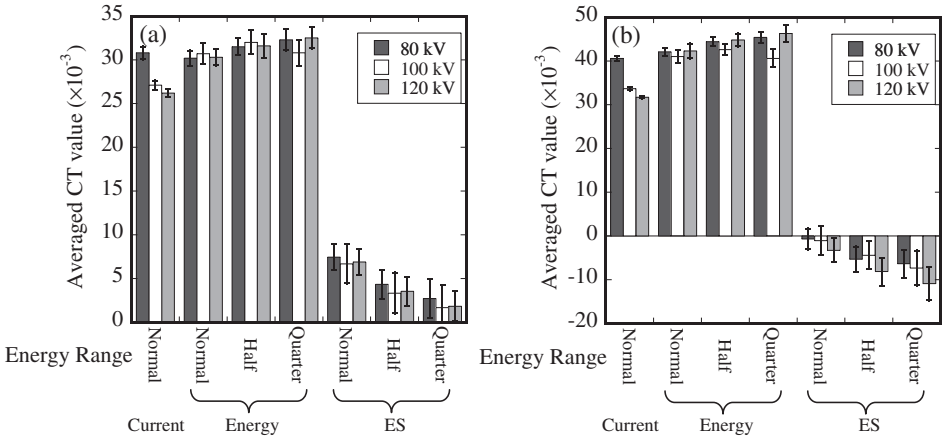

Fig. 10 Comparison of the averaged CT values obtained by the current-based CT, energy-based CT, and ES-based CT in the (a) acrylic and (b) iodine regions for each X-ray tube voltage. The normal columns show the CT values before the energy ranges were changed. The half and quarter columns show the CT values after the energy ranges were changed as described in Sec. V-1. Error bars show the standard deviations of the averaged CT values.

increased. Conversely, the energy-based and ES-based CT measurements had no such tendency.

6. Number of Segment Detectors

The effect of the number of segment detectors on the measured CT values was also considered. CT images and CT value profiles on the center line of the phantom acquired by two- and four-channel transXend detectors are shown in **Figs. 11** and **12**, respectively (the energy-based CT values were multiplied by -1 to allow comparison with Fig. 8). The transXend detector with four segment detectors was successfully applied both for energy-based and ES-based CT. With only two segment detectors, the energy-based CT gave tolerable CT values, while the ES-based CT was unsatisfactory.

The disappearance of the iodine region in the ES-based CT using a two-channel transXend detector was due to an insufficient change in the measured currents by the first and second segment detectors. Consequently, the resulting unfolded energy distribution was not correct.

7. Comparison between Si(Li) and CsI(Tl) Segment Detectors

As a substrate of the segment detector of a transXend detector, CsI(Tl) was compared with Si(Li). The CsI(Tl) array with photodiodes (S5668-11, Hamamatsu Photonics K. K., Japan) was employed for this purpose. Using the same scanning technique described in Sec. III-2, the cylindrical acrylic phantom was scanned with a six-channel CsI(Tl) transXend detector. The dimensions of each CsI(Tl) scintillator detector were 2 mm wide by 5.4 mm high and 1.2 mm thick. Regardless of the type of segment detectors, the phantom was translated once and the acquired data were duplicated 17 times so that the data were in 10 degree intervals, symmetric about the axis of the phantom. The CT values obtained with the CsI(Tl) and the Si(Li) transXend detectors are shown in **Fig. 13** (where the energy CT values were multiplied by -1 for clarity). For current-based CT using the Si(Li) segment detectors, the difference between the CT values in the acrylic region and in the iodine region was larger than the one with the CsI(Tl) segment detectors since a greater number of high-energy X-rays, which have a lower probability of being attenuated by iodine, passed through the Si(Li) detector than through the CsI(Tl) detector. A form of the beam hardening effect was occurring within the CsI(Tl) detectors. For the energy-based and ES-based CT measurements, the Si(Li) segment detector had the advantage that the fluctuations of CT values were small. The CsI(Tl) segment detectors opposite the side of X-ray incidence experienced less X-ray interactions since each CsI(Tl) scintillator absorbed more X-rays than Si(Li).

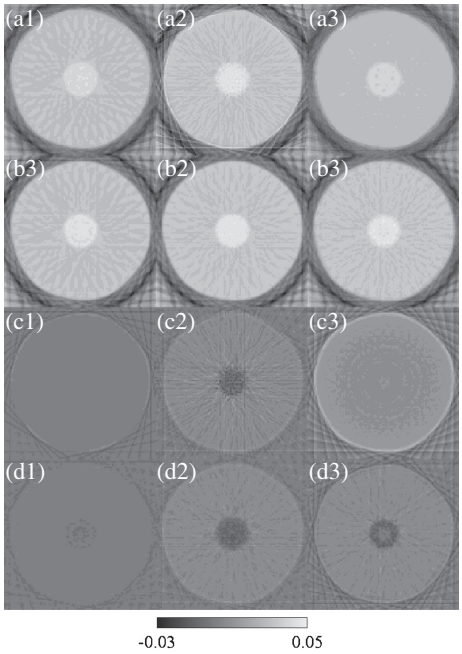

Fig. 11 CT images acquired by two- and four-channel transXend detectors. (a, b) Energy-based and (c, d) ES-based CT images. The numbers of segment detectors were (a, c) two and (b, d) four. X-ray tube voltages were (1) 80, (2) 100, and (3) 120 kV.

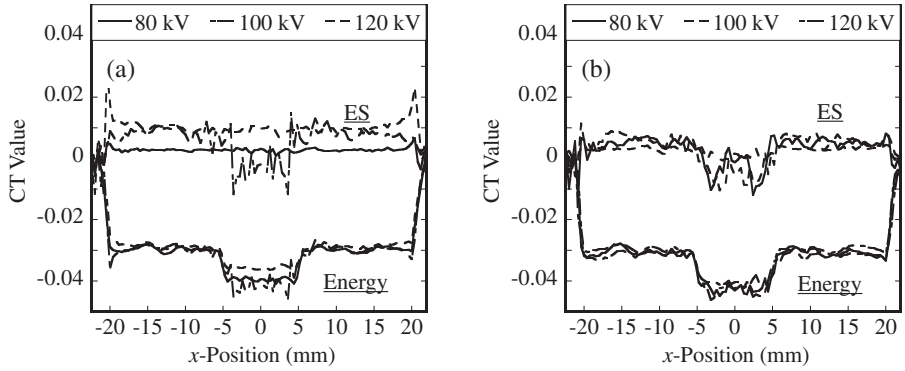

Fig. 12 CT value profiles on the center line of the phantom of the energy-based and ES-based CT images measured using (a) two-channel and (b) four-channel transXend detectors (the energy CT values were multiplied by −1 for comparison with Fig. 8).

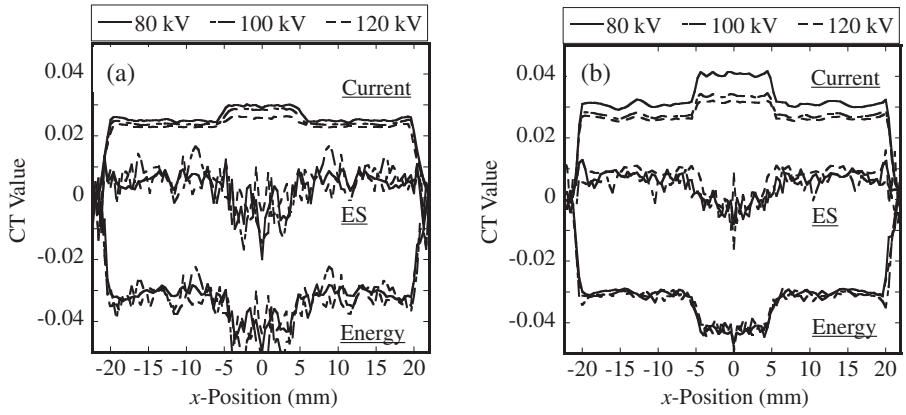

Fig. 13 Comparison between the CT value profiles on the center line of the phantom images measured by (a) CsI(Tl) and (b) Si(Li) transXend detectors (the energy-based CT values were multiplied by −1 for clarity).

Moreover, in the CsI(Tl) detector, less current was created due to the quantum efficiencies of scintillation creation and electron conversion at the photodiode. Therefore, in the current-based CT, the difference between the CT values in the acrylic region and in the iodine region was smaller.

VI. Conclusions

This paper demonstrated that it was necessary to use response functions designed for the acrylic thickness closest to the X-ray path length in the phantom. Using variable response functions in the unfolding process, the CT values for a homogeneous material were constant as were the CT measurement results detecting each X-ray.

It was also shown that the transXend detector enabled the acquisition of CT images independent of the X-ray tube voltage. This suggested that the transXend detector had an advantage over conventional current mode detectors, especially at higher X-ray tube voltages.

The CT value dependences on the energy range and the number of segment detectors were discussed. The transXend detector experiments had the significant advantage of offering many ways to analyze the same measurement data.

Si(Li) and CsI(Tl) transXend detectors were also compared. For the current-based CT using the transXend detector, higher contrast between the acrylic and iodine regions was achieved with the Si(Li) segment detector. In addition, the Si(Li) transXend detector had the advantage of producing smaller fluctuations in the measured CT values. However, it would be possible to improve the CT image quality acquired with a CsI(Tl) transXend detector by using a thinner CsI(Tl) scintillator.

Further consideration is necessary to determine the optimum thickness, number, and substrate material of the segment detectors.

Acknowledgments

The authors are very grateful to Prof. K. Hitomi, Tohoku University, for allowing them to use his CT image reconstruction program. This work was partly supported by a Grant-in-Aid for Scientific Research from the Japan Society for the Promotion of Science.

References

1) R. A. Brooks, G. Di Chiro, "Beam hardening in X-ray reconstructive tomography," *Phys. Med. Biol.*, **21**, 390–398 (1976).
2) I. Kanno, A. Uesaka, S. Nomiya, H. Onabe, "Energy measurement of X-rays in computed tomography for detecting contrast

media," *J. Nucl. Sci. Technol.*, **45**, 15–24 (2008).
3) I. Kanno, R. Imamura, K. Mikami, A. Uesaka, M. Hashimoto, M. Ohtaka, K. Ara, S. Nomiya, H. Onabe, "A current mode detector for unfolding X-ray energy distribution," *J. Nucl. Sci. Technol.*, **45**, 1165–1170 (2008).
4) I. Kanno, R. Imamura, K. Mikami, M. Hashimoto, M. Ohtaka, K. Ara, S. Nomiya, H. Onabe, "Energy subtraction computed tomography measured by current-mode detector," *Nucl. Instrum. Methods Phys. Res.*, **A610**, 325–327 (2009).
5) W. McElroy, S. Berg, T. Crocket, G. Hawkins, *A Computer Automated Iterative Method for Neutron Flux Spectra Determination for Foil Activation*, AFWL-TR-67-41 (1967).
6) E. Storm, "Calculated bremsstrahlung spectra from thick tungsten targets," *Phys. Rev.*, **A5**, 2328–2338 (1972).